AGU ADVANCING EARTH AND SPACE SCIENCE

Geophysical Research Letters

Key Points:

- Five-million-year records of terrestrial material input to the northwest shelf of Australia were investigated
- The records indicate a continuously Pliocene-Pleistocene drying trend in northwestern Australia
- More variable climates with less vegetation coverage and expanded desert/dune during the late Pleistocene were observed

Correspondence to:

Y. He and H. Wang,
yxhe@zju.edu.cn;
wanghy@ieecas.cn

Terrestrial Material Input to the Northwest Shelf of Australia Through the Pliocene-Pleistocene Period and Its Implications on Continental Climates

Yuxin He[1] ![ORCID] **and Huanye Wang[2]**

[1]Key Laboratory of Geoscience Big Data and Deep Resource of Zhejiang Province, School of Earth Sciences, Zhejiang University, Hangzhou, China, [2]State Key Lab of Loess and Quaternary Geology, Center for Excellence in Quaternary Science and Global Change, Chinese Academy of Sciences, Institute of Earth Environment, Xi'an, China

Abstract Based on biomarkers and bulk organic carbon isotope, we reconstructed a 5-million-year history of terrestrial material input to the northwest shelf of Australia. Vegetational organic input continuously decreased through the Pliocene-Pleistocene period due to decreased vegetation coverage and discharge under general aridification process. Triggered by lowered sea level and drier climates, soil input increased after ∼2.5–2.2 million years ago (Ma). Bulk terrestrial organic input demonstrates stronger variability after ∼1.7 Ma, as influenced by large-amplitude hydrological swings on the Australian continent. Source of soils shifted between ∼1.5 and 1.2 Ma, along with presence of active dune fields. All lines of evidence together indicate a general wet climate in northwestern Australia during the early Pliocene, a continuously drying trend to the mid-Pleistocene, and a drier phase with less vegetation coverage and expanded desert during the late Pleistocene, which is modulated by ongoing Indonesian Throughflow constriction and global atmospheric circulations.

Plain Language Summary Terrestrial material indicators recorded in nearshore marine sedimentary cores are useful for studying the continental climates in northwestern Australia. Here, we present biomarker-based data from cores at International Ocean Discovery Program Site U1461 to reconstruct the history of the terrestrial material input to the northwest shelf of Australia over the last 5 million years. We aim to reveal how the vegetation and soil organic transportations responded to climate changes in northwestern Australia through the Pliocene-Pleistocene period. Our results show a continuous decrease in the vegetational organic input since 5 million years ago (Ma), an increased soil input at ∼2.5–2.2 Ma, a stronger variability in bulk terrestrial organic input since ∼1.7 Ma, and a shift in soil source between ∼1.5 and 1.2 Ma. All these changes together indicate that the climates in northwestern Australia shifted from a generally wet condition during the early Pliocene to a drier and more variable phase during the late Pleistocene, which is controlled by ongoing Indonesian Throughflow constriction and global atmospheric circulations.

1. Introduction

The Australian continent has been predominantly influenced by the Indian Ocean circulations (Cane & Molnar, 2001; Molnar & Cronin, 2015; Schott et al., 2009; Sniderman et al., 2016), distinctive from the regions that were mainly controlled by the Northern Hemisphere glacial–interglacial oscillations (Haug et al., 1999). As an important component of the Indian Ocean thermohaline conveyor, the Indonesian Throughflow (ITF) transports water and heat from the western Pacific Ocean into the eastern Indian Ocean and provides a major water source for the shallow and narrow Leeuwin Current (LC, <100 km wide, <300 m deep) along the west shelf of Australia (Gordon, 2005). ITF variability regulates the poleward heat transport in the Indian Ocean and thus the moisture availability on the semiarid northwestern Australian continent (Molnar & Cronin, 2015). Constriction and reconnection of the ITF significantly modulate the monsoonal strength and thus the climates in western Australia region (Cane & Molnar, 2001; Herold et al., 2011; Krebs et al., 2011; Molnar & Cronin, 2015; Wyrwoll et al., 2009).

Through the Pliocene-Pleistocene period, the ITF constriction was induced by the emergence of the Maritime Continent due to both sea level lowering and tectonic reorganization of the Indonesian Gateway system (Cane & Molnar, 2001; Christensen et al., 2017; Krebs et al., 2011). Over the decades, the timing

and the climatic effect of the ITF constriction on the Australian continent have been investigated. Based on records from International Ocean Discovery Program (IODP) Sites U1459 and U1463, some major ITF constriction events during the Pliocene have been identified, including the one at ∼3.7 million years ago (Ma) triggered by a tectonic reorganization of the Maritime Continent and the one at ∼3.3 Ma induced by a quick sea level drop (Auer et al., 2019, 2020; Christensen et al., 2017; De Vleeschouwer et al., 2018, 2019; Smith et al., 2020). The restricted ITF and the synchronous cooling conditions have resulted in a major climatic transition to less moisture availability in northern and western Australia (Christensen et al., 2017; Molnar & Cronin, 2015; Sniderman, 2011; Sniderman et al., 2007, 2013, 2016; Stuut et al., 2019). The general aridification is accompanied by an expansion of C4 plants due to increased seasonality of precipitation from the onset of the Australian summer monsoon regime at ∼3.5 Ma, although the correlation between the ITF constriction and the onset of Australian monsoon still remains under debate (Andrae et al., 2018).

During the Pleistocene, the ITF remained tectonically restricted (Cane & Molnar, 2001; Krebs et al., 2011). Temperature records from Site U1463 based on glycerol dialkyl glycerol tetraethers (GDGTs) and long-chain diols show a strong cooling condition at ∼1.7–1.5 Ma, resulting from a stronger ITF constriction (Smith et al., 2020). Also, a GDGT-based temperature record at Site U1460 suggests cooling and weak ITF conditions at ∼0.65 Ma and ∼1.55 Ma, which were caused by lowering sea level and regional tectonic changes (Petrick et al., 2019). Temperature and primary productivity records at Site U1461 suggested prevailing warm, low-salinity, nutrient-deficient surface water, and thus a stronger LC under the restricted ITF after ∼1.2 Ma, tentatively suggesting a complex relation between the LC and the ITF (He et al., 2021). During the mid- to late Pleistocene with the weak ITF and the strong LC, a generally drier conditions in northwestern and southeastern Australia were recognized (McLaren & Wallace, 2010; Sniderman, 2011; Sniderman et al., 2016; Stuut et al., 2019). Besides, larger glacial-interglacial monsoonal oscillations become another important signature in the Australian area (Gallagher et al., 2009; Spooner et al., 2011). However, due to sparse records covering the Pliocene-Pleistocene period, how the continental environments evolved along with the ITF constriction and the general aridification remains elusive and requires further investigations.

Terrestrial vegetation and soil organic carbon (OC) transportations recorded in nearshore marine sedimentary cores are very useful for reconstructing continental climate (Andrae et al., 2018; Christensen et al., 2017; Smith et al., 2020; Stuut et al., 2019). Basically, vegetational OC reflects moisture availability for the vegetation to grow and discharge for the vegetational OC to be transported to marine environment (Hedges & Oades, 1997). Terrigenous soils that end up on the northwest shelf of Australia might be from both airborne dusts emitted during dry seasons and discharge-transported soils under strong hydrological condition during rainy seasons (Stuut et al., 2019). Biomarkers are powerful tools in disentangling terrestrial OC input to marine ocean. First, bulk OC isotope ($\delta^{13}C_{org}$) is indicative of bulk contribution of terrestrial OC, considering that OC of terrestrial origins contains more negative $\delta^{13}C_{org}$ values than those of aquatic sources (Hedges & Oades, 1997; Meyers, 1994). Second, long-chain *n*-alkanes are mainly sourced from vascular plants (Cranwell et al., 1987; Ficken et al., 2000). When normalized with oceanic primary productivity (e.g., C_{28-30} sterol, Volkman et al., 1998), they can track vegetational OC input. Third, terrigenous soils are characteristic by relatively high abundances of branched GDGTs (brGDGTs, Schouten et al., 2013; Weijers et al., 2007). The branched and isoprenoid tetraether (BIT, Hopmans et al., 2004) index is a good indicator of soil OC input to the shelf area (Schouten et al., 2013). Distribution of brGDGTs, expressed in the cyclization ratio of branched tetraethers (CBT) and the methylation index of branched tetraethers (MBT), describes soil OC under difference climatic settings in terms of temperature and pH values (Weijers et al., 2007).

In this study, we present biomarker-based records of terrestrial material input to the northwest shelf of Australia over the last 5 million years (Myr), based on sedimentary cores at Site U1461 drilled during IODP Expedition 356 (Figure 1). We aim to disentangle the responses of vegetation and dust transportation to climatic variations in the northwestern Australian continent through the Pliocene-Pleistocene period.

2. Materials and Methods

Site U1461 is located on the northwest shelf of Australia (20°12′51″S, 115°03′56″E, water depth of 126 m, Figure 1), ∼100 km northwest of the Barrow Island. Age-depth model for sedimentary cores at Site U1461 was built by integrating datums from biostratigraphy, micropaleontology, lithological property, and ^{14}C dates distributed from the top 950 m (Figure S1, see details in He et al., 2021).
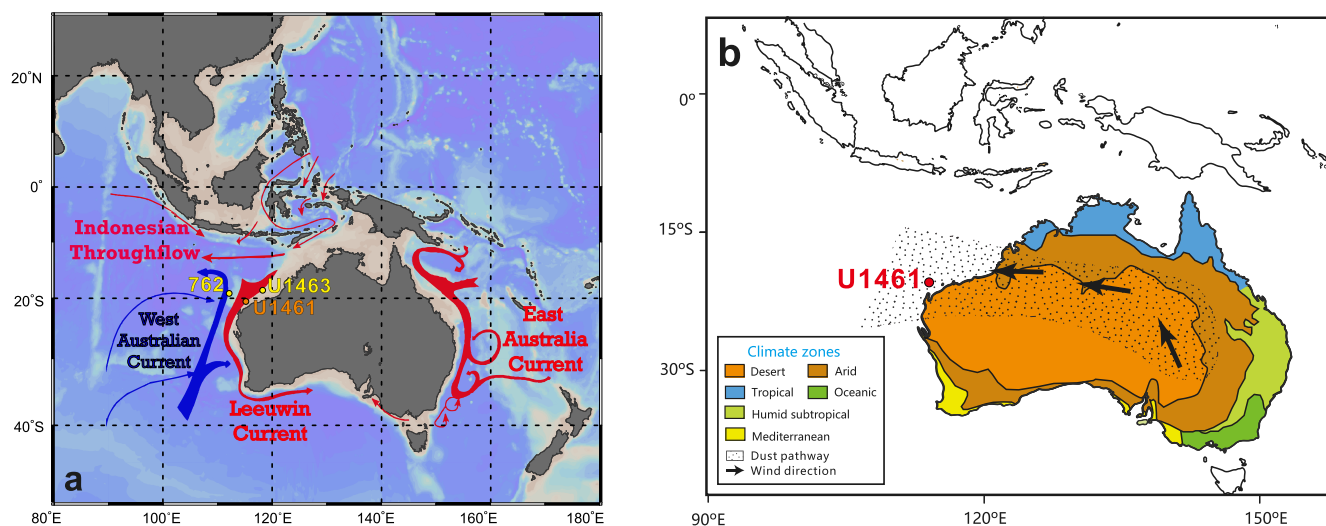
Figure 1. (a) Modern oceanography (created by the software of Ocean Data View), ocean circulations in the Indo-Pacific and Australian regions (adapted from Gallagher et al., 2009), and the positions of International Ocean Discovery Program (IODP) Sites U1461, U1463, and ODP 762. Warm and cold surface currents were shown in red and blue arrows. (b) Modern Australian climatic zones and dust pathway (adapted from Christensen et al., 2017).

Samples for $\delta^{13}C_{org}$ analysis ($n = 148$) were pretreated with 3 N HCl for 24 h to remove carbonates, rinsed with deionized water until the pH value becomes 7, and subsequently dried at 60°C. The carbonate-free samples were analyzed for $\delta^{13}C_{org}$ using a Thermo-Fisher FLASH 2000 Elemental Analyzer coupled with a MAT-253 Isotopic Ratio Mass Spectrometer. The 1σ precision for the $\delta^{13}C_{org}$ analysis is ±0.2‰.

For biomarker analysis, total lipids were ultrasonic extracted from ~20 g freeze-dried sediments ($n = 239$) with solvent of dichloromethane/methanol (9:1, v/v). The total lipids were then hydrolyzed with 6% KOH in methanol solution. Neutral fraction was extracted by n-hexane from the hydrolyzed lipids. The neutral fraction was analyzed on an Agilent 7890B Gas Chromatography-Flame Ionization Detector (Figure S2) for quantitation of n-C_{31} alkane and C_{28-30} sterols using both internal (n-$C_{24}D_{50}$) and external standards (cholesterol). After that, the neutral fraction was redissolved in hexane/isopropanol (99:1, v/v), filtered with 0.45 µm glass-fiber filter, and analyzed on a Shimadzu 8030 High-Performance Liquid Chromatography-Mass Spectrometry for quantification of GDGTs. Thirty-four chosen samples were further cleaned by silica-gel chromatography and analyzed for n-C_{16-33} alkanes (Figure S2).

The vegetational OC input was expressed by the $C_{31Alk}/C_{28-30Str}$ ratio, calculated as:

$$\frac{C_{31Alk}}{C_{28-30Str}} = \frac{\left[n - C_{31}\text{alkane}\right]}{\left(\left[C_{28}\text{sterol}\right] + \left[C_{29}\text{sterol}\right] + \left[C_{30}\text{sterol}\right]\right)}. \tag{1}$$

The BIT, MBT, and CBT values were calculated as:

$$BIT = \frac{\left(\left[Ia\right] + \left[IIa\right] + \left[IIIa\right]\right)}{\left(\left[Ia\right] + \left[IIa\right] + \left[IIIa\right] + \left[Cren\right]\right)}, \tag{2}$$

$$MBT = \frac{\left(\left[Ia\right] + \left[Ib\right] + \left[Ic\right]\right)}{\left(\left[Ia\right] + \left[Ib\right] + \left[Ic\right] + \left[IIa\right] + \left[IIb\right] + \left[IIc\right] + \left[IIIa\right] + \left[IIIb\right] + \left[IIIc\right]\right)}, \tag{3}$$

$$CBT = -\log\frac{\left[Ib\right] + \left[IIb\right]}{\left[Ia\right] + \left[IIa\right]}, \tag{4}$$
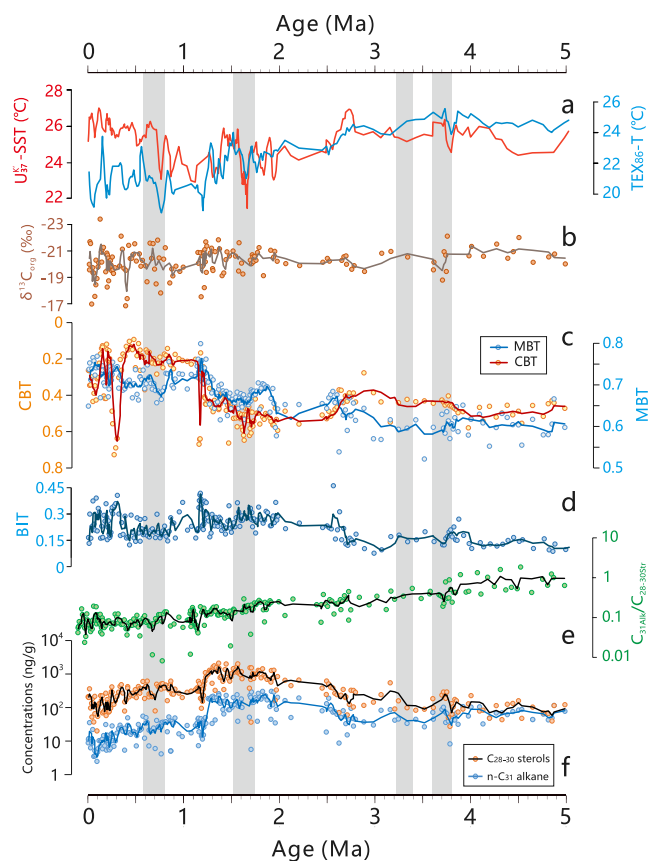
Figure 2. Terrestrial material input, temperatures, and primary productivity on the northwest shelf of Australia over the last 5 million years. (a) Three-point smoothed $U^{K'}_{37}$-based (red) and TEX_{86}-based (blue) temperatures (He et al., 2021). (b) $\delta^{13}C_{org}$ values with three-point smoothing curve. (c) Methylation index of branched tetraethers (MBT; blue) and cyclization ratio of branched tetraethers (CBT; orange) values with three-point smoothing curves. (d) Branched and isoprenoid tetraether (BIT) values with three-point smoothing curve. (e) $C_{31Alk}/C_{28-30Str}$ values with three-point smoothing curve. (f) Concentrations of C_{28-30} sterols (orange) and n-C_{31} alkane (blue) with three-point smoothing curves. Gray shadings indicate weak Indonesian Throughflow (ITF) events, including 0.8–0.6, 1.7–1.5, 2.7–2.5, and 3.7–3.4 Ma (Auer et al., 2019, 2020; Christensen et al., 2017; De Vleeschouwer et al., 2019; He et al., 2021; Petrick et al., 2019; Smith et al., 2020).

where [X] is concentration of X compound (Hopmans et al., 2004; Weijers et al., 2007).

3. Results

At Site U1461, concentrations of n-C_{31} alkane and C_{28-30} sterols vary from 2.5 to 306.0 ng/g and from 20.1 to 2114.9 ng/g over the last 5 Myr, respectively (Table S1 and Figure 2f). In terms of the ratio-based proxy, $C_{31Alk}/C_{28-30Str}$ values vary from 0.008 to 1.84 (Figure 2e) and show a general decreasing trend between 5 and 0.8 Ma ($r^2 = 0.65$, $n = 159$, $p < 0.05$). At some well-recognized cooling and ITF weakening periods through the Pliocene–Pleistocene period, including 1.7–1.5, 2.7–2.5, and 3.8–3.5 Ma, $C_{31Alk}/C_{28-30Str}$ values also slightly decreased (Figure 2, Auer et al., 2019, 2020; De Vleeschouwer et al., 2018, 2019; He et al., 2021; Petrick et al., 2019; Smith et al., 2020). Compared with those between 5 and 0.8 Ma, the $C_{31Alk}/C_{28-30Str}$ values show no obvious decreasing or increasing trend between 0.8 and 0 Ma. The BIT, CBT, and MBT values vary from 0.08 to 0.47, from 0.09 to 0.73, and from 0.52 to 0.80 over the last 5 Myr, respectively (Table S1 and Figure 2). The BIT record displays generally lower values at ~5–2.7 Ma and higher values after ~2.5 Ma (Figure 2d). The MBT and CBT values are general stable before 1.5 Ma but display a transition from higher CBT and lower MBT values to lower CBT and higher MBT values between ~1.5 and 1.2 Ma (Figure 2c). The $\delta^{13}C_{org}$ values vary from −23.4‰ to −16.8‰ over the last 5 Myr (Table S1 and Figure 2b). The $\delta^{13}C_{org}$ values are relatively stable between 5 and 1.7 Ma, except for a ~2‰ positive excursion at ~3.7 Ma. The $\delta^{13}C_{org}$ values are ~1‰ more positive between ~3.3 and 1.7 Ma than between ~5 and 3.7 Ma. Over the last ~1.7 Myr, the $\delta^{13}C_{org}$ values show much larger variation (~3–5‰) without obvious increasing or decreasing trend.

4. Discussion

4.1. Vegetational OC Input on the Northwest Shelf of Australia

Concentrations of n-C_{31} alkane could be applied as an indicator of vegetational OC input, considering that this compound is mainly derived from terrestrial vascular plants (Andrae et al., 2018; Cranwell et al., 1987; Ficken et al., 2000). Meanwhile, concentrations of C_{28-30} sterols are indicative of marine primary productivity (Volkman et al., 1998). For instance, brassicasterol (C_{28} sterol, Volkman et al., 1998) and dinosterol (C_{30} sterol, Volkman et al., 1998) represent the productivity of diatoms and dinoflagellates, respectively. Choice of sterol compounds for the proxy would have limited impacts on the reconstruction of the vegetational OC input on the northwest shelf of Australia, according to similar variation patterns in different ratios of long-chain n-alkanes versus sterols (e.g., C_{31Alk}/C_{28Str}, C_{31Alk}/C_{30Str}, and $C_{31Alk}/C_{28-30Str}$, Figure S3). Also, the $C_{31Alk}/C_{28-30Str}$ ratio shows independent variation with concentrations of C_{28-30} sterols (Figure 2), suggesting neglectable influence from the primary productivity on this ratio-based proxy. Third, the decreasing $C_{31Alk}/C_{28-30Str}$ signature roughly resembles another low-resolution vegetational OC record based on the ratios of long-chain versus short-chain n-alkanes (Figure S4, Ficken et al., 2000). Therefore, the $C_{31Alk}/C_{28-30Str}$ values are indicative of the vegetational OC input on the northwest shelf of Australia.

According to the $C_{31Alk}/C_{28-30Str}$ values, the vegetational OC input demonstrates a general decreasing trend from the early Pliocene to the mid-Pleistocene (5–0.8 Ma). Theoretically, sea level, vegetation coverage, and riverine discharge could be the major controllers on vegetational OC input. The global sea level started to de-

Figure 3. Compilation of terrestrial material input and climates of northwestern Australia over the last 5 million years. (a) Vegetational organic carbon input inferred by $C_{31Alk}/C_{28-30Str}$ values at Site U1461 (black, three-point smoothing). Mean annual precipitations in southern Australia based on Monte Carlo simulations on the continental vegetation change (red with 1σ error shadows, Sniderman et al., 2016). (b) $\delta^{13}C_{org}$ values at Site U1461 (brown, three-point smoothing). (c) Soil input inferred by uranium concentrations from Site U1463 (orange, Christensen et al., 2017) and BIT values from Site U1461 (dark blue, three-point smoothing) and Site U1463 (light blue, Smith et al., 2020). (d) Source of soils inferred by MBT and CBT values (three-point smoothed) from Site U1461. (e) River runoff and terrigenous input based on percentage of potassium (%K) from Site U1463 (blue, Auer et al., 2020; Christensen et al., 2017) and log(Fe/Ca) record from Site 762 (green, Auer et al., 2020; Stuut et al., 2019). (f) Global sea level record (blue, De Boer et al., 2010) derived from global benthic $\delta^{18}O$ records (Lisiecki & Raymo, 2005), and some local and global events including the onset of the Northern Hemispheric Glaciation (NHG), the mid-Pleistocene transition (MPT), and the MIS 50–60, 100, G2, and M2 events (green). Gray shadings indicate weak ITF events (same with Figure 2). A summary of terrestrial material input and climatic variations in northwestern Australia is shown at the bottom.

crease after ~3 Ma, moving Site U1461 closer to the shoreline (Figure 3d, De Boer et al., 2010). The concurring lower $C_{31Alk}/C_{28-30Str}$ values suggest that the sea level variation only exerts minor impact on the vegetational OC input to Site U1461. By contrast, the decreasing $C_{31Alk}/C_{28-30Str}$ values seem to mimic the long-term ITF constriction trend (Figure 2, Christensen et al., 2017). Also at periods with weak ITF conditions including 1.7–1.5, 2.7–2.5, and 3.7–3.4 Ma, the $C_{31Alk}/C_{28-30Str}$ record also suggests decreased vegetational OC input (Figure 2, Auer et al., 2019, 2020; Christensen et al., 2017; De Vleeschouwer et al., 2019; He et al., 2021; Petrick et al., 2019; Smith et al., 2020). Therefore, the decrease of the vegetational OC input between 5 and 0.8 Ma might be largely due to less discharge and less vegetation coverage in drier phases under the restricted ITF condition. Such hypothesis is further supported by lower river runoff and terrigenous input in northwestern Australia, as inferred from the concentrations of potassium from Site U1463 (Figure 3e, Auer et al., 2020; Christensen et al., 2017) and the log(Fe/Ca) record from ODP Site 762 (Figure 3e, Auer et al., 2020; Stuut et al., 2019). The $C_{31Alk}/C_{28-30Str}$ values remain in low values and do not show obvious decreasing pattern between 0.8 and 0 Ma. The apparent stable $C_{31Alk}/C_{28-30Str}$ values suggest generally dry conditions during the mid- and late Pleistocene.

4.2. Soil OC Input on the Northwest Shelf of Australia

The BIT record demonstrates generally higher values after ~2.5 Ma than those between ~5 and 2.5 Ma (mean of 0.25 vs. 0.15, Figures 3 and S5), suggesting higher terrigenous soil transportation (Hopmans et al., 2004; Schouten et al., 2013; Weijers et al., 2007, 2014). According to another BIT record at Site U1463, there are a short increase at 2.55 Ma and a long-term increase after 2.3 Ma (Figure 3, Smith et al., 2020). Also, the gamma radiation-derived uranium concentrations at Site U1463, which were recognized as a dust proxy considering the presence of uranium bearing rocks exposed on the northwest Australian continent, increased at ~2.4 Ma (Christensen et al., 2017). Considering the very low resolution in records at Site U1461 between 2.5 and 2.2 Ma (three points only), we reported the increased soil OC input at ~2.5–2.2 Ma, keeping in mind that the different timings of increased soil input can also be attributed to slightly different source materials and responses to climatic variability between Sites U1461 and U1463. The variation of soil OC input to the northwest shelf of Australia shows a complex relationship with that of vegetational OC input (Figure 2), suggesting different controlling factors on them. Terrigenous soil transportation to the northwest shelf of Australia is a mixture of signals from dust emitted during dry seasons, riverine discharge carrying soils during rainy seasons, and distance of the studied site to the shoreline (Stuut et al., 2019). Lower river runoff and moisture during the Pleistocene compared to the Pliocene has been widely observed in many records (Figure 3, Auer et al., 2020; Christensen et al., 2017; Stuut et al., 2019). Therefore, the increase in the soil OC input should be largely attributed to lower sea level and higher dust availability under dry conditions. As global sea level lowered after ~2.5 Ma (Figure 3, De Boer et al., 2010), Site U1461 moved closer to the shoreline, receiving more soils from the Australian continent. Also, when land cover conditions crossed a tipping point under dry climates, soil availability would become higher with increased area of desert and decreased vegetation coverage.

There is a transition from higher CBT and lower MBT values to lower CBT and higher MBT values between ~1.5 and 1.2 Ma (Figure 3). In terms of the calculated mean annual air temperature derived from Weijers et al. (2007), the soils occurring between 1.2 and 0 Ma contain warmer signals (27.3°C vs. 21.8°C, Figure S6), in contrasting with the recognition of globally cooler conditions during the mid- and late Pleistocene compared to those during the Pliocene (Brierley et al., 2009; Fedorov et al., 2013; Lisiecki & Raymo, 2005). Therefore, changes in the MBT and CBT values are rather attributed to a shift in the source of the terrestrial soils. Indeed, this shift in soil source between ~1.5 and 1.2 Ma is accompanied by an increase contribution of grasses over trees and shrubs, as inferred by the alkane C_{33}/C_{29} ratio (Figure S4, Meyers & Ishiwatari, 1993). Accordingly, the widespread formation and initiation of deserts and the degradation of trees and shrubs in the Australia continent at ~1.2 Ma (Fujioka & Chappell, 2010) could induce the exposure of soils from the desert that previously formed in warmer periods (maybe the Miocene, considering the soils are 5.5°C warmer than those in the Pliocene and the early Pleistocene).

4.3. Bulk Terrestrial OC Input on the Northwest Shelf of Australia

The $\delta^{13}C_{org}$ values are relatively stable between 5 and 1.7 Ma, except for a ~2‰ positive excursion at ~3.7 Ma, probably due to less terrestrial input under dry climates from the ITF restriction. Besides that, the $\delta^{13}C_{org}$ values are only ~1‰ more positive between ~3.3 and 1.7 Ma than between ~5 and 3.7 Ma (Figure 2). The continuously decreased vegetational OC input between 5 and 0.8 Ma would induce an increasing effect on the $\delta^{13}C_{org}$ values at Site U1461 (Figure 2e). The percentage of C4 plants over C3 plants increased by ~20% between 5 and 1.7 Ma (Andrae et al., 2018), also resulting in an increase in the vegetation $\delta^{13}C_{org}$ values (~3‰). To the contrary, the increased soil OC input at ~2.5–2.2 Ma would to some extent lower the overall terrestrial $\delta^{13}C_{org}$ values (Figure 2). Complex interactions among these factors might result in relatively stable $\delta^{13}C_{org}$ values.

Over the last ~1.7 Myr, the $\delta^{13}C_{org}$ values show no obvious increasing or decreasing trend but larger variation (~3–5‰), suggesting a period of occasional massive and limited terrestrial transportations (Figure 2b). No correlations of $C_{31Alk}/C_{28-30Str}$ versus $\delta^{13}C_{org}$ ($r^2 = 0.0078$, $n = 102$, $p = 0.42$) and BIT versus $\delta^{13}C_{org}$ ($r^2 = 0.0025$, $n = 98$, $p = 0.66$) were observed over the last ~1.7 Myr. It is possible that very complicated sources and transport processes together resulted in the complex relations among the three proxies through the Pliocene-Pleistocene period (Figure 3). Nevertheless, the $\delta^{13}C_{org}$ values still add another dimension of the terrestrial OC story, by suggesting fragile environments with large-amplitude hydrological swings. Over the late Pleistocene, large glacial-interglacial oscillations and strong sea level variations become important climatic signatures in northwestern Australia (Auer et al., 2021; Gallagher et al., 2009; Spooner et al., 2011; Stuut et al., 2019). This is perhaps the reason for large-amplitude hydrological swings on the Australian continent at orbital scales, signaling the larger variation in the $\delta^{13}C_{org}$ values after the mid-Pleistocene transition (MPT, ~1.2 Ma).

4.4. Implications of the Terrestrial Records on the Continental Climates

In summary, the $C_{31Alk}/C_{28-30Str}$ values at Site U1461 are indicative of riverine transportation and vegetation coverage impacted by general changes in moisture. The BIT values reflect soil and dust OC input, induced mainly by sea level variation and partly by dry climates. The $\delta^{13}C_{org}$ values provide an indication of bulk terrestrial OC versus primary productivity, which could be influenced by very complicated sources and transport processes. These records clearly show a continuously decreased vegetational OC input since 5 Ma, an increased soil input at ~2.5–2.2 Ma, stronger variability in the bulk terrestrial OC input after ~1.7 Ma, and a shift in soil source between ~1.5 and 1.2 Ma. Different proxies show their particular responses and sensitivities to climatic variabilities. Generally, vegetation records are more sensitive to wet and moderate dry climates, whereas soil records are more indicative of much drier conditions. For instance, between ~1.5 and 1.2 Ma when the soil source shifted along with presence of active dune fields, the climates were too dry to show any drastic vegetation changes, and the vegetational OC inputs do not show obvious decreasing patterns (Figure 3).

All the terrestrial records together indicate that northwestern Australia continuously became drier through the Pliocene-Pleistocene period, from generally wet during the early Pliocene, to very variable and dry

conditions during the late Pleistocene (Figure 3). The phenomena seen in northwestern Australia are also observed throughout Australia. For instance, in central Australia, vegetations more indicative of wetter conditions were found during the early Pliocene (Figure 3a; Sniderman et al., 2016), while the presence of active dune fields initiated at ~1 Ma (Fujioka & Chappell, 2010). In southeastern Australia, records from upland paleolakes in the semiarid interior indicated the persistence of strong rainfall until 1.5–1.4 Ma (McLaren & Wallace, 2010; McLaren et al., 2011; Sniderman et al., 2013).

During the Pliocene, the restricted ITF and the synchronous cooling conditions have resulted in a major climatic transition to lower moisture availability in northwestern Australia (Christensen et al., 2017; Molnar & Cronin, 2015; Sniderman, 2011; Sniderman et al., 2007, 2013, 2016; Stuut et al., 2019). Although the Earth also experienced a global cooling trend through the Pliocene, the ITF variability is slightly different from the global climatic signatures. For instance, the major ITF constriction occurred at ~3.7 Ma, prior to the temperature decrease in the offshore area (~3.5 Ma, Karas et al., 2011) and the stronger glacial events (Figure 3f, De Vleeschouwer et al., 2019; Smith et al., 2020). Also, sea surface temperatures on the northwest shelf of Australia are relatively higher during the onset of the Northern Hemispheric Glaciation (NHG) at 2.73 Ma (He et al., 2021; Smith et al., 2020). Therefore, the regional behavior instead of the global one is the major contributor to the ITF constriction and temperature variation in northwestern Australia. During the Pleistocene, the increased aridity in northwest Australian continent may be caused by both the ITF restriction and the global atmospheric circulations (Christensen et al., 2017; He et al., 2021; Smith et al., 2020). Further ITF constriction and shallowing of the Indonesian Gateway at ~1.7–1.5 Ma might trigger the more variable climates (Smith et al., 2020). As the meridional temperature contrast increased and the Hadley cell intensified since the MPT, a stronger atmospheric subsidence would increase the aridification in northwestern Australia (Fedorov et al., 2013).

5. Conclusions

The terrestrial records from Site U1461 show a continuously decreasing vegetational OC input since 5 Ma and intermittently increased soil input at ~2.5–2.2 Ma. Accordingly, we confirm wet conditions during the early Pliocene period and a continuously drying trend through the Pliocene-Pleistocene period, leading to less vegetation coverage, less river discharge, and higher soil availability. The continued tectonic northward migration of Australia and related restriction of the ITF pathways through the Indonesian Archipelago likely drove a reduction in moisture on the Australian continent. The records also demonstrate stronger variability in the bulk terrestrial OC input after ~1.7 Ma, as well as a shift in soil source between ~1.5 and 1.2 Ma. We further suggest drier and more variable conditions with less vegetation coverage and expanded desert/dune in northwestern Australia began at the mid- and late Pleistocene, largely induced by further ITF constriction and global atmospheric circulations.

Data Availability Statement

All data presented in this manuscript are available in Zenodo (https://doi.org/10.5281/zenodo.4500066).

References

Andrae, J. W., McInerney, F. A., Polissar, P. J., Sniderman, J. M. K., Howard, S., Hall, P. A., & Phelps, S. R. (2018). Initial expansion of C4 vegetation in Australia during the late Pliocene. *Geophysical Research Letters*, *45*, 4831–4840. https://doi.org/10.1029/2018GL077833

Auer, G., De Vleeschouwer, D., & Christensen, B. A. (2020). Towards a robust Plio-Pleistocene chronostratigraphy for ODP Site 762. *Geophysical Research Letters*, *47*, e2019GL085198. https://doi.org/10.1029/2019GL085198

Auer, G., De Vleeschouwer, D., Smith, R. A., Bogus, K., Groeneveld, J., Grunert, P., et al. (2019). Timing and pacing of Indonesian Throughflow restriction and its connection to late Pliocene climate shifts. *Paleoceanography and Paleoclimatology*, *34*, 635–657. https://doi.org/10.1029/2018PA003512

Auer, G., Petrick, B., Yoshimura, T., Mamo, B. L., Martinez-Garcia, A., Takayanagi, H., et al. (2021). Intensified organic carbon burial on the Australian shelf after the Middle Pleistocene Transition. *Quaternary Science Reviews*, *262*, 106965. https://doi.org/10.1016/j.quascirev.2021.106965

Brierley, C. M., Fedorov, A. V., Liu, Z., Herbert, T. D., Lawrence, K. T., & LaRiviere, J. P. (2009). Greatly expanded tropical warm pool and weakened Hadley circulation in the early Pliocene. *Science*, *323*, 1714–1718. https://doi.org/10.1126/science.1167625

Cane, M. A., & Molnar, P. (2001). Closing of the Indonesian seaway as a precursor to east African aridification around 3–4 million years ago. *Nature*, *411*, 157–162. https://doi.org/10.1038/35075500

Christensen, B. A., Renema, W., Henderiks, J., De Vleeschouwer, D., Groeneveld, J., Castañeda, I. S., et al. (2017). Indonesian Throughflow drove Australian climate from humid Pliocene to arid Pleistocene. *Geophysical Research Letters*, *44*, 6914–6925. https://doi.org/10.1002/2017GL072977

Cranwell, P. A., Eglinton, G., & Robinson, N. (1987). Lipids of aquatic organisms as potential contributors to lacustrine sediments—II. *Organic Geochemistry*, *11*, 513–527. https://doi.org/10.1016/0146-6380(87)90007-6

De Boer, B., van de Wal, R. S. W., Bintanja, R., Lourens, L. J., & Tuenter, E. (2010). Cenozoic global ice-volume and temperature simulations with 1-D ice-sheet models forced by benthic $\delta^{18}O$ records. *Annals of Glaciology*, *51*, 23–33. https://doi.org/10.3189/172756410791392736

De Vleeschouwer, D., Gerald, A., Rebecca, S., Kara, B., Beth, C., Jeroen, G., et al. (2018). The amplifying effect of Indonesian Throughflow heat transport on late Pliocene Southern Hemisphere climate cooling. *Earth and Planetary Science Letters*, *500*, 15–27. https://doi.org/10.1016/j.epsl.2018.07.035

De Vleeschouwer, D., Petrick, B. F., & Martínez-García, A. (2019). Stepwise weakening of the Pliocene Leeuwin Current. *Geophysical Research Letters*, *46*, 8310–8319. https://doi.org/10.1029/2019GL083670

Fedorov, A. V., Brierley, C. M., Lawrence, K. T., Liu, Z., Dekens, P. S., & Ravelo, A. C. (2013). Patterns and mechanisms of early Pliocene warmth. *Nature*, *496*, 43–49. https://doi.org/10.1038/nature12003

Ficken, K. J., Li, B., Swain, D. L., & Eglinton, G. (2000). An *n*-alkane proxy for the sedimentary input of submerged/floating freshwater aquatic macrophytes. *Organic Geochemistry*, *31*, 745–749. https://doi.org/10.1016/s0146-6380(00)00081-4

Fujioka, T., & Chappell, J. (2010). History of Australian aridity: Chronology in the evolution of arid landscapes. *Geological Society, London, Special Publications*, *346*, 121–139. https://doi.org/10.1144/sp346.8

Gallagher, S. J., Wallace, M. W., Li, C. L., Kinna, B., Bye, J. T., Akimoto, K., et al. (2009). Neogene history of the West Pacific Warm Pool, Kuroshio and Leeuwin Currents. *Paleoceanography*, *24*, PA1206. https://doi.org/10.1029/2008PA001660

Gordon, A. L. (2005). Oceanography of the Indonesian seas and their throughflow. *Oceanography*, *18*, 14–27. https://doi.org/10.5670/oceanog.2005.01

Haug, G. H., Sigman, D. M., Tiedemann, R., Pedersen, T. F., & Sarntheink, M. (1999). Onset of permanent stratification in the subarctic Pacific Ocean. *Nature*, *401*, 21–24. https://doi.org/10.1038/44550

He, Y., Wang, H., & Liu, Z. (2021). Development of the Leeuwin Current on the northwest shelf of Australia through the Pliocene-Pleistocene period. *Earth and Planetary Science Letters*, *559*, 116767. https://doi.org/10.1016/j.epsl.2021.116767

Hedges, J. I., & Oades, J. M. (1997). Comparative organic geochemistries of soils and marine sediments. *Organic Geochemistry*, *27*, 319–361. https://doi.org/10.1016/s0146-6380(97)00056-9

Herold, N., Huber, M., Greenwood, D. R., Müller, R. D., & Seton, M. (2011). Early to middle Miocene monsoon climate in Australia. *Geology*, *39*, 3–6. https://doi.org/10.1130/g31208.1

Hopmans, E. C., Weijers, J. W. H., Schefuß, E., Herfort, L., Sinninghe Damsté, J. S., & Schouten, S. (2004). A novel proxy for terrestrial organic matter in sediments based on branched and isoprenoid tetraether lipids. *Earth and Planetary Science Letters*, *224*, 107–116. https://doi.org/10.1016/j.epsl.2004.05.012

Karas, C., Nürnberg, D., Tiedemann, R., & Garbe-Schönberg, D. (2011). Pliocene Indonesian Throughflow and Leeuwin Current dynamics: Implications for Indian Ocean polar heat flux. *Paleoceanography*, *26*, PA2217. https://doi.org/10.1029/2010PA001949

Krebs, U., Park, W., & Schneider, B. (2011). Pliocene aridification of Australia caused by tectonically induced weakening of the Indonesian Throughflow. *Palaeogeography, Palaeoclimatology, Palaeoecology*, *309*, 111–117. https://doi.org/10.1016/j.palaeo.2011.06.002

Lisiecki, L. E., & Raymo, M. E. (2005). A Pliocene–Pleistocene stack of 57 globally distributed benthic $\delta^{18}O$ records. *Paleoceanography*, *20*, PA1003. https://doi.org/10.1029/2004PA001071

McLaren, S., & Wallace, M. W. (2010). Plio-Pleistocene climate change and the onset of aridity in southeastern Australia. *Global and Planetary Change*, *71*, 55–72. https://doi.org/10.1016/j.gloplacha.2009.12.007

McLaren, S., Wallace, M. W., Gallagher, S. J., Miranda, J. A., Holdgate, G. R., Gow, L. J., et al. (2011). Palaeogeographic, climatic and tectonic change in southeastern Australia: The late Neogene evolution of the Murray Basin. *Quaternary Science Reviews*, *30*, 1086–1111. https://doi.org/10.1016/j.quascirev.2010.12.016

Meyers, P. A. (1994). Preservation of elemental and isotopic source identification of sedimentary organic matter. *Chemical Geology*, *114*, 289–302. https://doi.org/10.1016/0009-2541(94)90059-0

Meyers, P. A., & Ishiwatari, R. (1993). Lacustrine organic geochemistry an overview of indicators of organic matter sources and diagenesis in lake sediments. *Organic Geochemistry*, *20*, 867–900. https://doi.org/10.1016/0146-6380(93)90100-p

Molnar, P., & Cronin, T. W. (2015). Growth of the Maritime Continent and its possible contribution to recurring ice ages. *Paleoceanography*, *30*, 196–225. https://doi.org/10.1002/2014PA002752

Petrick, B., Martínez-García, A., Auer, G., Reuning, L., Auderset, A., Deik, H., et al. (2019). Glacial Indonesian Throughflow weakening across the mid-Pleistocene Climatic Transition. *Scientific Reports*, *9*, 16995. https://doi.org/10.1038/s41598-019-53382-0

Schott, F. A., Xie, S., & McCreary, J. P. (2009). Indian Ocean circulation and climate variability. *Reviews of Geophysics*, *47*, RG1002. https://doi.org/10.1029/2007RG000245

Schouten, S., Hopmans, E. C., & Sinninghe Damsté, J. S. (2013). The organic geochemistry of glycerol dialkyl glycerol tetraether lipids: A review. *Organic Geochemistry*, *54*, 19–61. https://doi.org/10.1016/j.orggeochem.2012.09.006

Smith, R. A., Castañeda, I. S., Groeneveld, J., De Vleeschouwer, D., Henderiks, J., Christensen, B. A., et al. (2020). Plio-Pleistocene Indonesian Throughflow variability drove Eastern Indian Ocean sea surface temperatures. *Paleoceanography and Paleoclimatology 35*, e2020PA003872. https://doi.org/10.1029/2020PA003872

Sniderman, J. M. K. (2011). Early Pleistocene vegetation change in upland south-eastern Australia. *Journal of Biogeography 38*, 1456–1470. https://doi.org/10.1111/j.1365-2699.2011.02518.x

Sniderman, J. M. K., Jordan, G. J., & Cowling, R. M. (2013). Fossil evidence for a hyperdiverse sclerophyll flora under a non-Mediterranean type climate. *Proceedings of the National Academy of Sciences of the United States of America*, *110*, 3423–3428. https://doi.org/10.1073/pnas.1216747110

Sniderman, J. M. K., Pillans, B., O'Sullivan, P. B., & Kershaw, A. P. (2007). Climate and vegetation in southeastern Australia respond to Southern Hemisphere insolation forcing in the late Pliocene-Early Pleistocene. *Geology*, *35*, 41–44. https://doi.org/10.1130/g23247a.1

Sniderman, J. M. K., Woodhead, J. D., Hellstrom, J., Jordan, G. J., Drysdale, R. N., Tyler, J. J., et al. (2016). Pliocene reversal of late Neogene aridification. *Proceedings of the National Academy of Sciences of the United States of America*, *113*, 1999–2004. https://doi.org/10.1073/pnas.1520188113

Spooner, M. I., De Deckker, P., Barrows, T. T., & Fifield, L. K. (2011). The behaviour of the Leeuwin Current offshore NW Australia during the last five glacial–interglacial cycles. *Global and Planetary Change*, *75*, 119–132. https://doi.org/10.1016/j.gloplacha.2010.10.015

Stuut, J. B. W., De Deckker, P., Saavedra-Pellitero, M., Bassinot, F., Drury, A. J., Walczak, M. H., et al. (2019). A 5.3-million-year history of monsoonal precipitation in northwestern Australia. *Geophysical Research Letters*, *46*, 6946–6954. https://doi.org/10.1029/2019GL083035

Volkman, J. K., Barrett, S. M., Blackburn, S. I., Mansour, M. P., Sikes, E. L., & Gelin, F. (1998). Microalgal biomarkers: A review of recent research developments. *Organic Geochemistry*, *29*, 1163–1179. https://doi.org/10.1016/s0146-6380(98)00062-x

Weijers, J. W. H., Schefuß, E., Kim, J. H., Sinninghe Damsté, J. S., & Schouten, S. (2014). Constraints on the sources of branched tetraether membrane lipids in distal marine sediments. *Organic Geochemistry*, *72*, 14–22. https://doi.org/10.1016/j.orggeochem.2014.04.011

Weijers, J. W. H., Schouten, S., van den Donker, J. C., Hopmans, E. C., & Sinninghe Damsté, J. S. (2007). Environmental controls on bacterial tetraether membrane lipid distribution in soils. *Geochimica et Cosmochimica Acta*, *71*, 703–713. https://doi.org/10.1016/j.gca.2006.10.003

Wyrwoll, K. H., Greenstein, B. J., Kendrick, G. W., & Chen, G. (2009). The palaeoceanography of the Leeuwin Current: Implications for a future world. *Journal of the Royal Society of Western Australia*, *92*, 37–51.